Geophysical Research Letters

RESEARCH LETTER
10.1029/2023GL105977

Tropical Cyclone Supercell Response to the Coast Using a Climatology of Radar-Derived Azimuthal Shear

A. Addison Alford[1,2], Andrew Messersmith[3], Bruce Pollock[3], Quentin Thomas[3], Thea N. Sandmæl[1,2], and Benjamin A. Schenkel[1,2,3]

[1]NOAA/OAR National Severe Storms Laboratory, Norman, OK, USA, [2]Cooperative Institute for Severe and High-Impact Weather Research and Operations, University of Oklahoma, Norman, OK, USA, [3]School of Meteorology, University of Oklahoma, Norman, OK, USA

Key Points:

- Tropical cyclone supercells are more likely to intensify as they move across the coastal boundary
- Radar-measured mesocyclone intensity increases very near and onshore in storms that produced tornadoes
- Changes in the near-coastal wind profile likely augments near-shore convergence and/or vertical wind shear

Supporting Information:

Supporting Information may be found in the online version of this article.

Correspondence to:

A. A. Alford,
addison.alford@noaa.gov

Citation:

Alford, A. A., Messersmith, A., Pollock, B., Thomas, Q., Sandmæl, T. N., & Schenkel, B. A. (2023). Tropical cyclone supercell response to the coast using a climatology of radar-derived azimuthal shear. *Geophysical Research Letters*, *50*, e2023GL105977. https://doi.org/10.1029/2023GL105977

Received 18 AUG 2023
Accepted 17 OCT 2023

Abstract Supercells in landfalling tropical cyclones (TCs) often produce tornadoes that can cause fatalities and extensive damage. In previous studies, many tornadoes have been shown to form <50 km from the coast, and their parent storms may also intensify as they cross the coastal boundary. This study uses WSR-88D observations of TC tornadic mesocyclones from 2011 to 2018 to examine changes in their low-level rotation upon moving onshore. We will show that radar-derived azimuthal shear tends to increase in storms that cross the coastal boundary. Similar intensification trends are also found in radar-derived (supercell) storm-scale divergence, such that storm-scale convergence increases as storms move onshore. It is likely changes in the near-coast vertical wind shear and/or near-shore convergence helps explain supercell intensification, which is important to consider particularly in operational settings.

Plain Language Summary Tornadoes often occur in the outer regions of tropical cyclones (TCs), and can cause extensive damage. Prior studies have shown that tornadoes form very near the coast as their parent storms intensify. However, observations of such processes are limited. This study explores this idea by examining 8 years of radar-observed tornadic storms to see how the parent storm's rotation responds as it crosses the coastal boundary. We show that storms that cross the coastal boundary generally intensify as they cross the coast, suggesting that the changes in the TC wind field structure between ocean and land augment storm intensity and the likelihood of tornadoes just inland of the coast.

1. Background

Supercells in the outer bands of tropical cyclones (TCs) are known to produce tornadoes, severe winds, and enhanced precipitation (Brauer et al., 2022; Edwards, 2012; Rappaport, 2014). The United States National Weather Service issues tornado warnings to the public using a variety of tools to monitor TC supercells, including environmental monitoring (e.g., with upper air radiosondes) and mesocyclone structure using Doppler weather radar (e.g., the United States Weather Surveillance Radar—1988 Doppler or WSR-88Ds, Crum & Alberty, 1993). Using radiosonde data can help to diagnose the environments of small, low-topped TC supercells (often termed "miniature" supercells) by characterizing the vertical structure of the atmosphere, which form in environments characterized by weak buoyancy and high vertical wind shear (VWS, Baker et al., 2009; McCaul, 1991; McCaul & Weisman, 2001; Morin & Parker, 2011). Miniature supercells have been observed by ground-based weather radar (Green et al., 2011; Spratt et al., 1997) and airborne Doppler radar (Eastin & Link, 2009), but on a limited basis compared to studies of supercells in the United States Great Plains.

TC tornadoes are known to preferentially form in the right front quadrant of TCs relative to storm motion (e.g., Baker et al., 2009; Gentry, 1983) and/or in the downshear right quadrant (i.e., to right of and in the direction of the synoptic-scale deep-tropospheric VWS vector; Schenkel et al., 2020). While tornadoes can occur well inland, previous studies found that a large proportion of tornadoes occurred within 50 km of the coast (Hill et al., 1966; Schenkel et al., 2021; Schultz & Cecil, 2009). A high fraction of TC tornadoes near the coast are typically weak (Enhanced Fujita/Fujita Scale 0–1 intensity) and occur <200 km from the center of the TC.

Environments with strong VWS and enhanced environmental buoyancy were favored in environmental studies of TC tornadoes and supercells (Baker et al., 2009; Carroll-Smith et al., 2019; Curtis, 2004; Green et al., 2011; McCaul, 1991; McCaul & Weisman, 1996, 2001) and can be maximized on varying scales. Buoyancy has been shown to be locally maximized on the scale of rainbands in several of the aforementioned studies via

midtropospheric dry air intrusions (e.g., Baker et al., 2009; Curtis, 2004) and on the scale of the coast via thermodynamic contrasts between ocean and land (e.g., Knupp et al., 2006). In terms of VWS, synoptic scale VWS acting upon the TC can be an organization mechanism for convection and enhance total VWS (Schenkel et al., 2021). On smaller scales, near-coast boundaries or convergence zones (e.g., coastal front) along coastlines can enhance (supercell) storm relative helicity (SRH, Curtis, 2004; Green et al., 2011; Knupp et al., 2006). Likewise, the change in surface roughness may cause the rapid reduction in the low-level TC winds. As such, VWS likely increases as the near-shore hurricane boundary layer adjusts to the increase in inland surface roughness (Alford et al., 2020; Hirth et al., 2012).

Understanding individual storm responses to changes in their mesoscale environment is important operationally. As VWS may be enhanced along the coast, TC mesocyclones may be expected to intensify as they move from ocean to land. Several studies have shown case-by-case evidence of low-level mesocyclones intensifying as they cross the coastal boundary. For example, Eastin and Link (2009) used near-coast WSR-88D observations to document three supercells as they crossed from ocean to land. Of the three storms, two produced tornadoes just inland, while showing increases in low-level reflectivity and rotation. Likewise, Green et al. (2011) showed that the mid-level radar-observed mesocyclone of four supercells was strongest as the supercells moved onshore associated with 50% increases in 0–1-km VWS shear over land compared to water. The increased shear was hypothesized to be the result of enhanced surface friction over land, consistent with the results of Alford et al. (2020).

Based on the studies above, it is unclear how mesocyclones generally behave as they cross the coastal boundary. While evidence points to a more favorable VWS environment as storms cross the coastal boundary, it is unclear how individual mesocyclones respond. In this study, we leverage single-Doppler observations in 8 years of TC tornado data to explore the intensity trends of supercell mesocyclones as they cross the coastal boundary. We specifically seek to understand if TC supercells intensify as they cross the coast from ocean to land. Understanding how supercells interact with the near-coastal environment is potentially useful to improving operational forecasts and warnings, which have high false alarm ratios (Martinaitis, 2017; Nowotarski et al., 2021).

2. Data and Methods

2.1. Storm Identification and Tracking

In this study, TC tornadoes reported between 2011 and 2018 were examined. TC tornado location and timing data were obtained from the Storm Prediction Center TC tornado database (Edwards & Mosier, 2022). Only tornadoes between 2011 and 2018 were examined in this study. TC tornadoes were cross-referenced with WSR-88D 0.5°-tilt data to determine the parent mesocyclone associated with each tornado report for cases within radar range. Cases where tornado reports could not be cross-referenced with WSR-88D data were corrected to find the appropriate storm and correct the location or timing error in the tornado database. Once a parent storm was identified, storms were manually tracked up to an hour prior to tornadogenesis using radar reflectivity and Doppler velocity information where possible (i.e., some storms formed less than an hour prior to tornadogenesis). In total 230 supercells were identified and are hereafter referred to as "pre-tornadic storms" documented in Sandmæl et al. (2023). Pre-tornadic storms that produced multiple tornadoes were separated by tornado.

2.2. Radar-Derived Quantities

The subjectively identified pre-tornadic storms were further examined objectively. First, azimuthal shear (commonly referred to as "AzShear") was computed from dealiased (Jing & Wiener, 1993; Losey-Bailor et al., 2019; Zittel, 2019) radar Doppler radial velocity data at the 0.5°-radar tilt following the method of Mahalik et al. (2019). AzShear is a linear, least squares azimuthal derivative of the Doppler velocity that approximates to one-half of the vertical vorticity (the other ∼half is unobserved in the radial dimension). AzShear is also computed using an inverse-range-dependent kernel to compensate for beam broadening and is used to quantify mesocyclone intensity (Sandmæl et al., 2023; Smith et al., 2016). Second, the manually identified pre-tornadic storm tracks were refined by locating the nearest AzShear maximum and recorded in space and time. In total, 2,355 AzShear maxima data points were recorded as a function of all pre-tornadic storm tracks. Third, the AzShear data were normalized using the lifetime-maximum AzShear for each pre-tornadic track (i.e., each tornado produced by a storm is considered as a separate track segment). A value of 1.0 indicates the point at which the AzShear for each pre-tornadic track point was at its maximum. Finally, the locations of the AzShear maxima were calculated as a function of distance from the

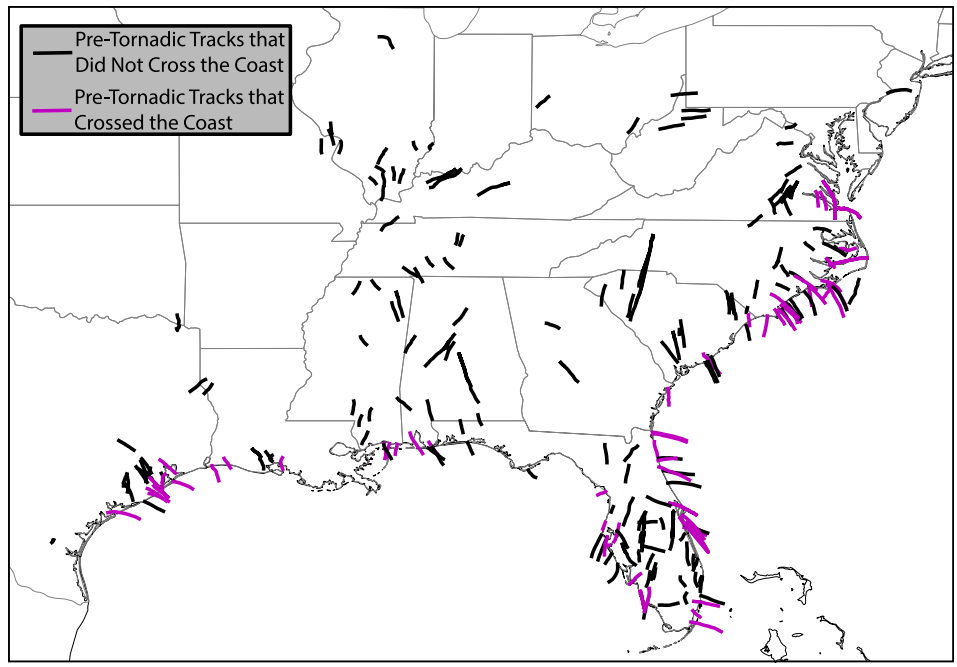

Figure 1. Tropical cyclone pre-tornadic tracks near the coast employed in this study, as well from the broader study period. Tracks specifically identified to have crossed the coastal boundary with valid radial velocity data both on- and off-shore are drawn in magenta (see Section 4). The remaining tracks in the data set are shown in black.

coast. The geographic data used to calculate distance from the coast were taken from the Global Self-consistent, Hierarchical, High-Resolution Geography Database with a horizontal grid spacing of ~1 km (Wessel & Smith, 1996).

Similar to AzShear, the radial gradient of Doppler velocity yields the divergent component of the radar-observed flow, where AzShear approximates the shear of the horizontal wind. Through a similar linear, least squares derivative, the divergence of the Doppler velocity is computed and hereafter referred to as "DivShear" (Mahalik et al., 2019). For reference, negative and positive values of DivShear are associated with convergence and divergence, respectively. DivShear data were normalized by the *minimum* lifetime DivShear for each pre-tornadic track. A value of 1.0 indicates the point at which Doppler velocity-inferred divergence was at a minimum (or convergence was at maximum). We employ DivShear here to gauge how the low level updraft responds near the coast, since trends in low level divergence can be used as a proxy for updraft intensity trends.

3. Examining Supercells That Crossed the Coastal Boundary

3.1. Pre-Tornadic Storm Tracks

As found in the climatological study of Schenkel et al. (2021), tornadoes were often favored near the coast. Here, we briefly examine the locations of storm tracks in our data set of pre-tornadic supercells (Figure 1), of which the cases herein are a subset of the data used in the Schenkel et al. (2021) study. In Figure 1, pre-tornadic supercell tracks are distributed across the eastern half of the United States. Tracks can be seen both well inland (e.g., >100 km from the coast; 63 supercells) or near the coast (e.g., <100 km from the coast; 167 cases). In general, it appears that tracks that are well inland are typically less dense than those confined to the coast, similar to the larger climatological signal seen in prior work (Schenkel et al., 2021; Schultz & Cecil, 2009).

Cases of note can be discerned from the map such as the high number of tornadoes produced by Hurricane Harvey in 2017 near Galveston Bay and Houston, TX. We point these out in particular, as a majority of the supercell tracks in each of these particular cases appear to be largely confined to near the coast and do not proceed well inland.

3.2. An Intensifying Supercell During Hurricane Harvey (2017)

We first examine a supercell that formed over the Gulf of Mexico and moved onshore into Texas during Hurricane Harvey. Harvey, a prolific tornado producer (Nowotarski et al., 2021), spawned tornadoes near the coastline,

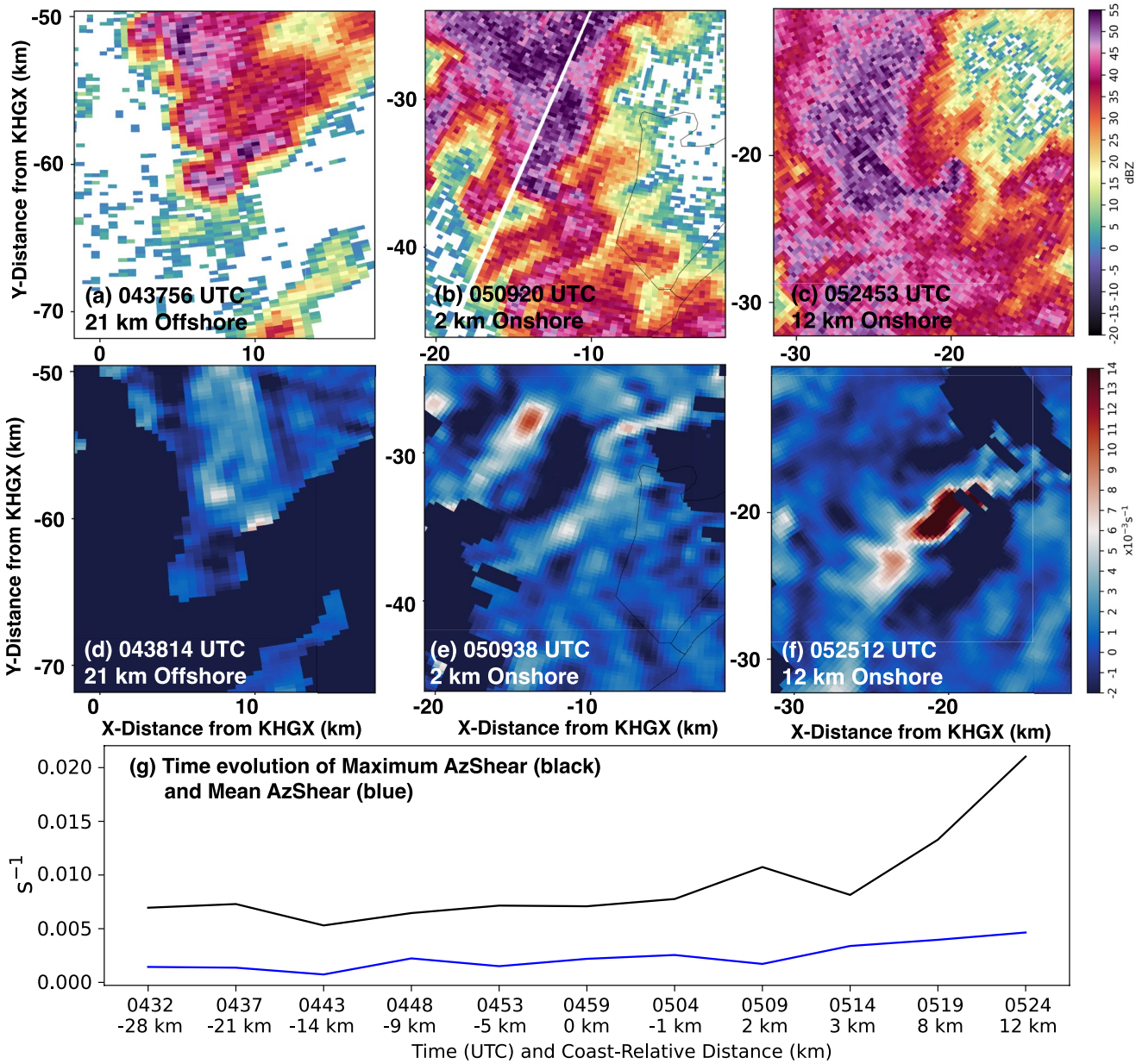

Figure 2. The radar presentation of a supercell in Hurricane Harvey is shown. The top row shows radar reflectivity, and the bottom row shows AzShear. The distance of the AzShear maximum from the coastline is shown by text in each panel. In (a, d), the supercell was 21 km offshore. In (b, e), the supercell had just made landfall, indicated by the thin black line showing the coastal boundary. In (c, f), the supercell was 12 km inland at which point it produced a tornado. (g) Shows the time-evolution maximum AzShear (black line) and mean AzShear (blue line) of the supercell observed prior to tornadogenesis. The coast-relative distance is indicated in the *x*-axis (negative distance is offshore).

where supercells within a quasi-stationary rainband formed over the Gulf of Mexico and moved onshore (Brauer et al., 2020). In Figure 2, we examine the radar presentation of one supercell that was observed by the WSR-88D in Houston (KHGX), which is generally representative of many of the supercells in this data set. At approximately 04:38 UTC (Figures 2a and 2d), the reflectivity and AzShear structure can be viewed respectively when the supercell was 21 km offshore. While reflectivity near the hook-like echo on the southern portion of the supercell approaches 55 dBZ, AzShear is just on the verge of intense rotation (that is, AzShear >0.006 s^{-1} which is a strong radar-based indication of tornado following Sandmæl et al. (2023)). Later at about 05:09 UTC, the supercell was moving onshore and began showing a classic supercell-like appearance. Specifically, a hook echo in reflectivity can been seen on the southern side of the cell ($x = -12$ km, $y = -36$ km in Figure 2b). Likewise, the AzShear

began increasing with values exceeding 0.006 s^{-1} (Figure 2d). As it moved inland at 05:25 UTC (Figures 2c and 2f), the supercell produced a tornado. The storm continued to be characterized by a hook echo in reflectivity and intensified in terms of AzShear. In Figure 2g, the evolution of the maximum and area mean AzShear is displayed at all radar times prior to tornado formation. Over water prior to 05:09 UTC, relatively little intensification was noted in either the maximum or mean AzShear. However, after landfall at 05:09 UTC, the maximum and mean AzShear generally increased until tornadogenesis at 05:24 UTC.

3.3. Offshore Peaks in AzShear

Not every pre-tornadic storm in the data set intensified solely over land, although many did. Waterspouts cannot be confirmed offshore, but they likely do exist (Edwards, 2012). For example, we show a pre-tornadic storm in Hurricane Florence (2018) that displayed similar radar-derived characteristics offshore and onshore. In Figure 3, a pre-tornadic storm observed by the WSR-88D in Wilmington, NC (KLTX) is shown. The storm is first identified 31 km offshore (Figures 3a and 3d) and does not resemble a classic supercell-like structure as in Figure 2. However, the AzShear in Figure 3d exceeds 0.01 s^{-1}, strongly indicative of an ongoing tornado (Sandmæl et al., 2023). While over water, the storm was strongest near 22:47 UTC (Figure 3g), but weakened as it approached the coastline. It reached a local minimum in intensity later near 23:06–23:07 UTC (Figures 3b and 3e). As it neared the coast, the storm intensified again between 23:06 and 23:13 UTC and spawned a tornado onshore. In terms of reflectivity, the cell obtained a hook echo-like feature visible on the southeastern periphery of the storm (e.g., near $x = 60$ km, $y = 38$ km in Figure 3c). AzShear increased further near landfall and again exceeded 0.01 s^{-1}. Similar to past studies (Baker et al., 2009; Spratt et al., 1997), the storm examined here was overall quite small in size (on the order of 10 km or less), making completely resolving its structure quite difficult by weather radar.

4. AzShear Relative to the Coast

In the previous section, we examined two pre-tornadic supercell storms in Hurricanes Harvey and Florence. Regardless of their offshore evolution, both storms intensified as they crossed the coastal boundary. Similar trends were noted in many other pre-tornadic storms in the data set. Other studies have found similar intensification trends with supercells crossing from ocean to land (Baker et al., 2009). We therefore explore this hypothesis by leveraging all pre-tornadic storms described in Section 2.

In order to examine how the pre-tornadic storms responded to the coast, we take a subset of the 230 pre-tornadic described in Section 2. Specifically, only storms that crossed the coastal boundary (regardless of how many tornadoes they produced) are herein examined. Some storms were tracked exclusively offshore, as the final radar observation prior to tornadogenesis was taken while the mesocyclone was just offshore. Such cases are not considered due to a lack of radar (AzShear) observations onshore. In total, 59 of the 230 storms crossed the coast (the magenta tracks in Figure 1) and produced 69 tornadoes. Of the 69 tornadoes, the normalized AzShear observations were at maximum (AzShear = 1) onshore in 40 of the 69 pre-tornadic tracks. Of the 29 that peaked in AzShear offshore, 17 were associated with peaks within 5 km of the coast, suggesting that few storms peaked in intensity well offshore. Similar to Schultz and Cecil (2009) and Alford et al. (2020), we bin the AzShear and DivShear observations in 10-km bins relative to the coast (positive distance is inland). The results are shown in Figure 4 for all pre-tornadic tracks (Figures 4a and 4b), pre-tornadic tracks where a tornado was produced <10 km inland (Figures 4c and 4d) and pre-tornadic tracks where a tornado was produced >10 km inland (Figures 4e and 4f).

In Figures 4a and 4b, the distributions of normalized AzShear and DivShear, respectively, are shown. From ocean to land, the median normalized AzShear and normalized DivShear tend to increase, consistent with Baker et al. (2009). The lowest and highest median normalized AzShear occur at a coast-relative distance of −45 km and +25 km, respectively. Likewise, the lowest median normalized DivShear occurs at −45 km, but the highest occurs at a range of +15 km. Again, from ocean to land the distributions of normalized AzShear shift toward higher values indicating that the cells achieve their highest values near the coast or inland. Specifically, the distributions at −45 and −35 km are skewed toward weaker values, indicating that AzShear is generally weaker over water in the cases sampled (we show in Section 5 and the supplemental material that this observation is likely not an effect of radar range). The distributions over water appear more evenly distributed around the median, and the

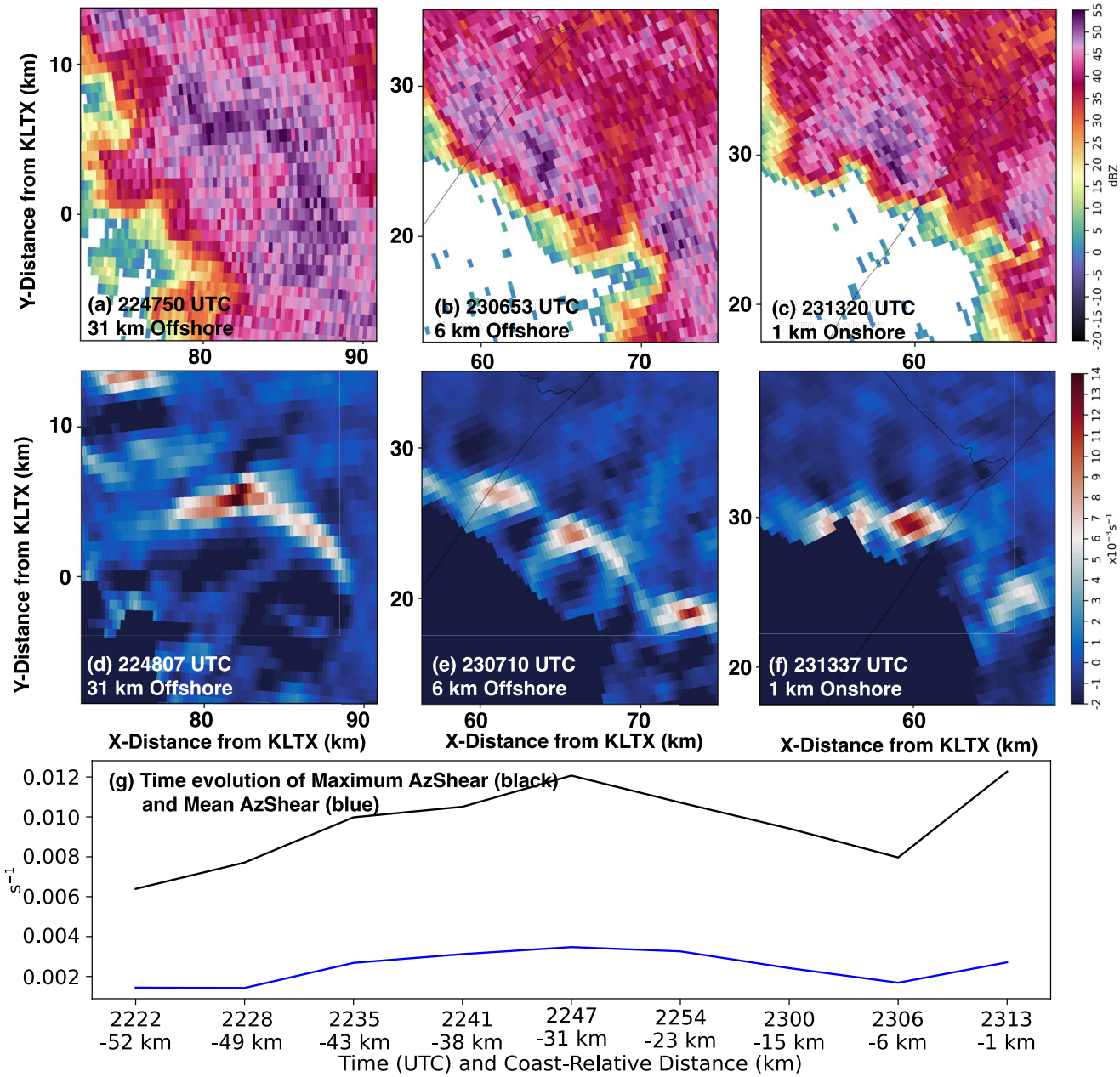

Figure 3. As in Figure 2, but for a supercell in Hurricane Florence (2018).

distributions over land tend to be shifted toward higher values. Similar trends in the distributions in DivShear from ocean to land can also be seen. Both the upward shift in the median and the distribution of AzShear appear to begin at the −5 km bin, indicating that storms may begin to intensify as they near the coastline.

We further examined the distributions between −20 and 0 km offshore (i.e., combining the distributions from the −15 and −5 km bins in Figure 4a to ensure statistically meaningful samples) and between 0 and +20 km onshore (i.e., combining the distributions from the +5 and + 15 km bins in Figure 4a). To examine statistical significance, we computed Kolmogorov-Smirnov (KS) tests using SciPy (Virtanen et al., 2020) and found that the change in AzShear as the storm moves onshore is statistically significant with a p-value of 0.0057. We also explored changes by limiting the distributions to within 10 km and widening the distributions to include all observations within 30 km of the coast. In those tests, we found p-values of 0.0001 and 0.0016, respectively, suggesting these results are insensitive to bin width. In addition to examining the statistical difference in the two on- and off-shore

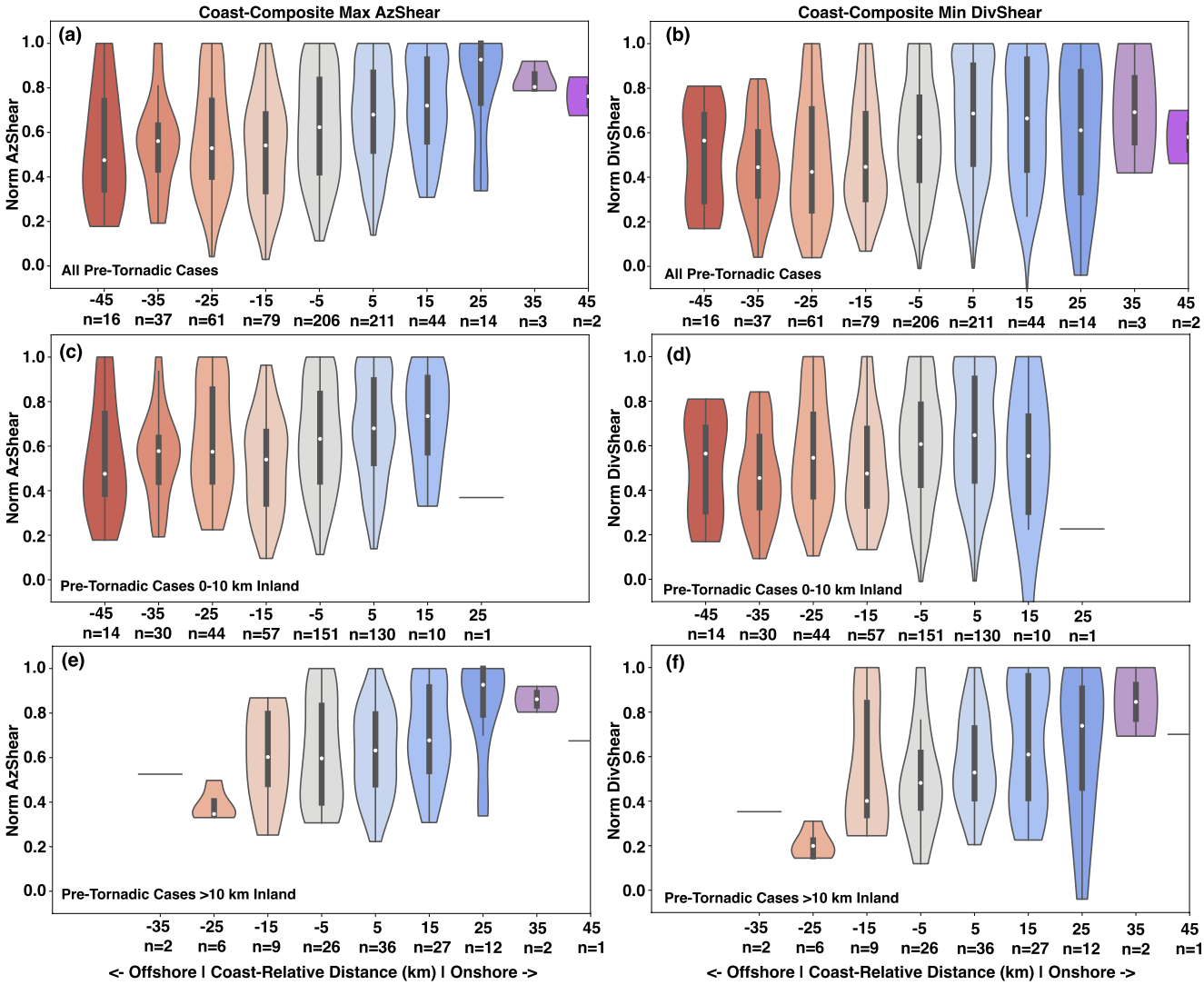

Figure 4. Violin plots of normalized AzShear and normalized DivShear for pre-tornadic storms that crossed the coastal boundary. The top row shows the coast-relative distributions of (a) normalized AzShear and (b) normalized DivShear for all storms that crossed the coast. The middle row (c, d) shows the same, but for pre-tornadic storms that produced tornadoes within 10-km inland. The bottom row (e, f) shows the same, but for pre-tornadic storms that produced tornadoes greater than 10-km inland. In the violin plots, the white dot is the median, the thick black bars denote the inner quartile range, the lower whisker denotes the lowest datum above the first quartile minus the interquartile range, and the upper whisker denotes the highest datum above the first quartile plus the interquartile range. Note that the 1.5× quartile range line is limited between 0 and 1 for AzShear and −1 and 1 for DivShear.

distributions, we computed the 95% confidence interval (CI) around the median using bootstrapping (10,000 samples) with re-sampling. We found that the medians of the −20–0 and 0–20-km distributions (0.54–0.64 and 0.65–0.73, respectively) were significantly different at the 95% CI. We likewise performed the same statistical tests for the distributions of normalized DivShear. As with AzShear, we combined the −15 and −5 km (+5 and +15 km) bins to represent offshore (onshore) observations. The *p*-value for the DivShear KS-test was 0.0009.

We further subset the pre-tornadic tracks by those that produced tornadoes <10 km inland (Figures 4c and 4d) and >10 km inland (Figures 4e and 4f). Not surprisingly, the differences in both the median normalized AzShear and median normalized DivShear follow those from all pre-tornadic cases. Specifically, the maximum normalized AzShear and maximum normalized DivShear is located in the 15 km onshore and 5 km range bins, respectively, suggesting that pre-tornadic storms often intensify as they move inland. Pre-tornadic storms that produced tornadoes deeper inland tended to begin intensifying deeper inland (i.e., in the +15 km range bin) in terms of the median normalized AzShear (Figure 4e). In terms of normalized DivShear, the storms show a similar response to the all cases and <10 km categories where the median DivShear begins increasing at the +5 km bin. We again

used the KS-test to compare the distributions of normalized AzShear and normalized DivShear offshore and onshore using the same methods as described previously. For pre-tornadic storms that produced tornadoes <10 km, we found small p-values (<0.05) similar to those computed from using all cases for both AzShear and DivShear distributions. Similarly, the 95% CI of the medians were also significantly different (0.54–0.64 offshore vs. 0.65–0.75 onshore). For pre-tornadic storms that produced tornadoes >10 km inland, we did not find statistical significance between the off- and on-shore distributions for the KS or median tests, although there were significantly fewer data points particularly in the offshore bins.

5. Summary and Discussion

This manuscript has examined pre-tornadic storms from 2011 to 2018. In particular, we examined the evolution of storms that formed offshore and moved across the coastal boundary. In general, we found that the mesocyclone intensity in storms tended to increase as storms moved onshore at which point they were more likely to produce a tornado. As such, this manuscript may suggest that near coastal influences such as the frictional adjustment of the low-level TC winds exerts influence on the environments through which pre-tornadic storms are moving.

In general, the synoptic-scale environment does not solely explain the high number of tornadoes at the coast (Schenkel et al., 2021). In this manuscript, however, we leverage the coast-relative framework to examine how the mesoscale changes in the VWS anticipated near and inland of the coast may impact individual storms. We note that the coast-relative changes in VWS and convergence is the subject of an ongoing investigation by the authors. The maximum normalized AzShear and DivShear quantities examined here are measures of the mesocyclone intensity in pre-tornadic TC supercells. Indeed we find that the mesocyclones in cells that cross the coastal boundary often intensify rapidly within 0–20 km of the coastline. There also appears to be an increase in mesocyclone intensity just offshore (e.g., the −5 km range bin in Figure 4), suggesting that the mesoscale environmental changes along the coast may partly extend over the ocean. Studies such as Knupp et al. (2006) and Green et al. (2011) discuss thermodyanmic and kinematic boundaries along the coast, respectively. Such boundaries may yield supercell intensification offshore, whereas the frictional effects of the boundary layer transition (Alford et al., 2020) may be more influential onshore. Additional observations are likely needed to more completely explain the intensification of storms just offshore.

We further sub-divided storms by the coast-relative location where they produced tornadoes (Figures 4c and 4f). Cells that produced tornadoes deeper inland intensified as they moved onshore, similar to those that produced tornadoes closer to the coast. Hence, the storm-scale intensification response appears to be related to the storm crossing the coastal boundary, rather than solely related to the storm producing a tornado.

This data set cannot verify that tornadoes did not occur offshore. However, we examined the intensity of mesocyclones offshore in those storms that produced a tornado onshore (e.g., Figure 3). In individual cases, we did find similar AzShear values in storms over the ocean. Since each of these pre-tornadic storms is over the ocean prior to tornadogenesis (Figure 4a), we expected the distribution of normalized AzShear to remain approximately constant if tornadoes are occurring at the same frequency on- and offshore. We did not find such results. This data set may suggest that some cells are producing tornadoes offshore, but the mesocyclones in this data set tend to be more intense onshore. We also examined the radar-relative range dependence on AzShear observations (Figure S1) and found that our results are not biased by radar range.

Given that storms often intensify as they move onshore, this study augments the results of studies such as Eastin and Link (2009), Green et al. (2011), Morin and Parker (2011), and Alford et al. (2020). The former two studies showed that storms in case studies tended to intensify as they crossed the coastal boundary, which may be explained by near-coast changes in the boundary layer wind field. For example, the VWS may increase due to the low-level wind reduction due to an increase in aerodynamic surface roughness. Similarly, the reduction in near-coastal winds may enhance convergence in a narrow zone oriented parallel to the coast or induce a spinup of the TC supercell mesocyclones. As such, the results of this study suggest TC tornadoes are more likely in cells that are crossing the coastal boundary. From an operational and warning-decision perspective, this study highlights the need for forecasters to carefully monitor individual supercell or supercell-like structures in landfalling TCs. While such storms pose a threat regardless of their initial location, those that are moving onshore should be carefully monitored via weather radar. From a research perspective, the evolution of TC supercells and their environments are still poorly understood. Examining how the environmental shear and convergence, for example,

are translated to supercell mesocyclone intensification is a subject that likely should be explored through targeted mobile observations.

Data Availability Statement

Radar data were curated by NCEI and available at Amazon as part of the NOAA Big Data Partnership at: https://registry.opendata.aws/noaa-nexrad (Ansari et al., 2018).

The SPC TC tornado data used here can be found at Edwards (2021) and at https://www.spc.noaa.gov/exper/tctor/ (Edwards & Mosier, 2022).

Pre-tornadic track data can be found at Alford et al. (2023).

Pre-tornadic data were constructed using the NOAA Weather and Climate Toolkit, available at https://www.ncdc.noaa.gov/wct/.

Figures were made using Matplotlib, version 3.6.3 for Figure 1 (Caswell et al., 2023) and version 3.4.3 (Caswell et al., 2021) for Figures 2 and 3 and Figure S1.

Figure 4 was made using Seaborn, version 0.11.2, available at https://seaborn.pydata.org/ (Waskom, 2021).

Azimuthal shear and divergent shear data were computed using the Warning Decision Support System-Integrated Information software, available at http://www.wdssii.org/download.shtml (Lakshmanan et al., 2007).

Acknowledgments
AAA, TNS, and BAS were partially supported by the NOAA/Office of Oceanic and Atmospheric Research under the NOAA-University of Oklahoma Cooperative Agreement NA21OAR4320204, U.S. Department of Commerce. AAA was also supported by the Peter Lamb Postdoctoral Fellowship (also under NA21OAR4320204) and by the NOAA/OAR National Severe Storms Laboratory. BAS was supported by NSF AGS-2028151. AM, BP, and QT were supported by the University of Oklahoma School of Meteorology. We thank Lance Wood and one anonymous reviewer for their comments that improved this work.

References

Alford, A. A., Sandmael, T. N., & Schenkel, B. A. (2023). Data for "tropical cyclone supercell response to the coast using a climatology of radar-derived azimuthal shear" (version 1) [Dataset]. Zenodo. https://doi.org/10.5281/ZENODO.8264787

Alford, A. A., Zhang, J. A., Biggerstaff, M. I., Dodge, P., Marks, F. D., & Bodine, D. J. (2020). Transition of the hurricane boundary layer during the landfall of Hurricane Irene (2011). *Journal of the Atmospheric Sciences*, *77*(10), 3509–3531. https://doi.org/10.1175/jas-d-19-0290.1

Ansari, S., Del Greco, S., Kearns, E., Brown, O., Wilkins, S., Ramamurthy, M., et al. (2018). Unlocking the potential of NEXRAD data through NOAA's big data partnership. *Bulletin of the American Meteorological Society*, *99*(1), 189–204. https://doi.org/10.1175/BAMS-D-16-0021.1

Baker, A. K., Parker, M. D., & Eastin, M. D. (2009). Environmental ingredients for supercells and tornadoes within Hurricane Ivan. *Weather and Forecasting*, *24*(1), 223–244. https://doi.org/10.1175/2008WAF2222146.1

Brauer, N. S., Alford, A. A., Waugh, S. M., Biggerstaff, M. I., Carrie, G. D., Kirstetter, P. E., et al. (2022). Hurricane Laura (2020): A comparison of drop size distribution moments using ground and radar remote sensing retrieval methods. *Journal of Geophysical Research: Atmospheres*, *127*(16), e2021JD035845. https://doi.org/10.1029/2021JD035845

Brauer, N. S., Basara, J. B., Homeyer, C. R., McFarquhar, G. M., & Kirstetter, P. E. (2020). Quantifying precipitation efficiency and drivers of excessive precipitation in post-landfall hurricane Harvey. *Journal of Hydrometeorology*, *21*(3), 433–452. https://doi.org/10.1175/JHM-D-19-0192.1

Carroll-Smith, D. L., Dawson, L. C., & Trapp, R. J. (2019). High-Resolution real-data WRF modeling and verification of tropical cyclone tornadoes associated with hurricane Ivan (2004). *Electronic Journal Severe Storms Meteorology*, *14*(2), 1–36. https://doi.org/10.55599/ejssm.v14i2.72

Caswell, T. A., Droettboom, M., Lee, A., De Andrade, E. S., Hoffmann, T., Hunter, J., et al. (2021). matplotlib/matplotlib: Rel: v3.4.3 [Software]. Zenodo. https://doi.org/10.5281/ZENODO.5194481

Caswell, T. A., Lee, A., Droettboom, M., De Andrade, E. S., Hoffmann, T., Klymak, J., et al. (2023). matplotlib/matplotlib: Rel: v3.6.3 [Software]. Zenodo. https://doi.org/10.5281/ZENODO.7527665

Crum, T. D., & Alberty, R. L. (1993). The WSR-88d and the WSR-88d operational Support facility. *Bulletin of the American Meteorological Society*, *74*(9), 1669–1687. https://doi.org/10.1175/1520-0477(1993)074⟨1669:TWATWO⟩2.0.CO;2

Curtis, L. (2004). Midlevel dry intrusions as a factor in tornado outbreaks associated with landfalling tropical cyclones from the Atlantic and Gulf of Mexico. *Weather and Forecasting*, *19*(2), 411–427. https://doi.org/10.1175/1520-0434(2004)019<0411:mdiaaf>2.0.co;2

Eastin, M. D., & Link, M. C. (2009). Miniature supercells in an offshore outer rainband of hurricane Ivan (2004). *Monthly Weather Review*, *137*(7), 2081–2104. https://doi.org/10.1175/2009MWR2753.1

Edwards, R. (2012). Tropical cyclone tornadoes: A review of knowledge in research and prediction. *Electronic J Severe Storms Meteor*, *7*(6), 1–61. https://doi.org/10.55599/ejssm.v7i6.42

Edwards, R. (2021). United States tornado reports in landfalling tropical cyclones used in Paredes et al. (2021) (1.0) [Dataset]. 25th conference on severe local storms (SLS). https://doi.org/10.5281/zenodo.5719433

Edwards, R., & Mosier, R. M. (2022). Over a quarter century of TCTOR: Tropical cyclone tornadoes in the WSR-88D ERA. In *Proc., 30th conf. on severe local storms* (p. 171). Retrieved from https://ams.confex.com/ams/30SLS/meetingapp.cgi/Paper/407018

Gentry, R. C. (1983). Genesis of tornadoes associated with hurricanes. *Monthly Weather Review*, *111*(9), 1793–1805. https://doi.org/10.1175/1520-0493(1983)111⟨1793:GOTAWH⟩2.0.CO;2

Green, B. W., Zhang, F., & Markowski, P. (2011). Multiscale processes leading to supercells in the landfalling outer rainbands of Hurricane Katrina (2005). *Weather and Forecasting*, *26*(6), 828–847. https://doi.org/10.1175/WAF-D-10-05049.1

Hill, E., Malkin, W., & Schulz, W. (1966). Tornadoes associated with cyclones of tropical origin—Practical features. *Journal of Applied Meteorology and Climatology*, *5*(6), 745–763. https://doi.org/10.1175/1520-0450(1966)005<0745:tawcot>2.0.co;2

Hirth, B. D., Schroeder, J. L., Weiss, C. C., Smith, D. A., & Biggerstaff, M. I. (2012). Research radar analyses of the internal boundary layer over cape Canaveral, Florida, during the landfall of hurricane Frances (2004). *Weather and Forecasting*, *27*(6), 1349–1372. https://doi.org/10.1175/WAF-D-12-00014.1

Jing, Z., & Wiener, G. (1993). Two-dimensional dealiasing of Doppler velocities. *Journal of Atmospheric and Oceanic Technology*, *10*(6), 798–808. https://doi.org/10.1175/1520-0426(1993)010⟨0798:TDDODV⟩2.0.CO;2

Knupp, K. R., Walters, J., & Biggerstaff, M. (2006). Doppler profiler and radar observations of boundary layer variability during the landfall of tropical storm Gabrielle. *Journal of the Atmospheric Sciences*, *63*(1), 234–251. https://doi.org/10.1175/JAS3608.1

Lakshmanan, V., Smith, T., Stumpf, G., & Hondl, K. (2007). The warning decision Support system–integrated information. *Weather and Forecasting*, *22*(3), 596–612. https://doi.org/10.1175/WAF1009.1

Losey-Bailor, A., Zittel, W. D., & Jing, Z. (2019). *Improving Doppler velocity coverage on the WSR-88D by using low PRFs with 2DVDA* (Technical Report). NWS Radar Operations Center Applications Branch.

Mahalik, M. C., Smith, B. R., Elmore, K. L., Kingfield, D. M., Ortega, K. L., & Smith, T. M. (2019). Estimates of gradients in radar moments using a linear least squares derivative technique. *Weather and Forecasting*, *34*(2), 415–434. https://doi.org/10.1175/WAF-D-18-0095.1

Martinaitis, S. M. (2017). Radar observations of tornado-warned convection associated with tropical cyclones over Florida. *Weather and Forecasting*, *32*(1), 165–186. https://doi.org/10.1175/waf-d-16-0105.1

McCaul, E. (1991). Buoyancy and shear characteristics of hurricane-tornado environments. *Monthly Weather Review*, *119*(8), 1954–1978. https://doi.org/10.1175/1520-0493(1991)119%3C1954:BASCOH%3E2.0.CO;2

McCaul, E., & Weisman, M. L. (1996). Simulations of shallow supercell storms in landfalling hurricane environments. *Monthly Weather Review*, *124*(3), 408–429. https://doi.org/10.1175/1520-0493(1996)124<0408:SOSSSI>2.0.CO;2

McCaul, E., & Weisman, M. L. (2001). The sensitivity of simulated supercell structure and intensity to variations in the shapes of environmental buoyancy and shear profiles. *Monthly Weather Review*, *129*(4), 664–687. https://doi.org/10.1175/1520-0493(2001)129⟨0664:tsosss⟩2.0.co;2

Morin, M. J., & Parker, M. D. (2011). A numerical investigation of supercells in landfalling tropical cyclones. *Geophysical Research Letters*, *38*(10), 1–7. https://doi.org/10.1029/2011GL047448

Nowotarski, C. J., Spotts, J., Edwards, R., Overpeck, S., & Woodall, G. R. (2021). *Tornadoes in hurricane Harvey*. Weather and Forecasting. https://doi.org/10.1175/WAF-D-20-0196.1

Rappaport, E. N. (2014). Fatalities in the United States from Atlantic tropical cyclones: New data and interpretation. *Bulletin of the American Meteorological Society*, *95*(3), 341–346. https://doi.org/10.1175/BAMS-D-12-00074.1

Sandmæl, T. N., Smith, B. R., Reinhart, A. E., Schick, I. M., Ake, M. C., Madden, J. G., et al. (2023). The tornado probability algorithm: A probabilistic machine learning tornadic circulation detection algorithm. *Weather and Forecasting*, *38*(3), 445–466. https://doi.org/10.1175/WAF-D-22-0123.1

Schenkel, B. A., Coniglio, M., & Edwards, R. (2021). How does the relationship between ambient deep-tropospheric vertical wind shear and tropical cyclone tornadoes change between coastal and inland environments? *Weather and Forecasting*, *36*(2), 539–566. https://doi.org/10.1175/WAF-D-20-0127.1

Schenkel, B. A., Edwards, R., & Coniglio, M. (2020). A climatological analysis of ambient deep-tropospheric vertical wind shear impacts upon tornadoes in tropical cyclones. *Weather and Forecasting*, *35*(5), 2033–2059. https://doi.org/10.1175/WAF-D-19-0220.1

Schultz, L. A., & Cecil, D. J. (2009). Tropical cyclone tornadoes, 1950-2007. *Monthly Weather Review*, *137*(10), 3471–3484. https://doi.org/10.1175/2009MWR2896.1

Smith, T. M., Lakshmanan, V., Stumpf, G. J., Ortega, K. L., Hondl, K., Cooooper, K., et al. (2016). Multi-radar multi-sensor (MRMS) severe weather and aviation products: Initial operating capabilities. *Bulletin of the American Meteorological Society*, *97*(9), 1617–1630. https://doi.org/10.1175/BAMS-D-14-00173.1

Spratt, S. M., Sharp, D. W., Welsh, P., Sandrik, A., Alsheimer, F., & Paxton, C. (1997). A WSR-88D assessment of tropical cyclone outer rainband tornadoes. *Weather and Forecasting*, *12*(3), 479–501. https://doi.org/10.1175/1520-0434(1997)012<0479:awaotc>2.0.co;2

Virtanen, P., Gommers, R., Oliphant, T. E., Haberland, M., Reddy, T., Cournapeau, D., et al. (2020). SciPy 1.0: Fundamental algorithms for scientific computing in Python. *Nature Methods*, *17*(3), 261–272. https://doi.org/10.1038/s41592-019-0686-2

Waskom, M. L. (2021). Seaborn: Statistical data visualization. *Journal of Open Source Software*, *6*(60), 3021. https://doi.org/10.21105/joss.03021

Wessel, P., & Smith, W. H. (1996). A global, self-consistent, hierarchical, high-resolution shoreline database. *Journal of Geophysical Research*, *101*(B4), 8741–8743. https://doi.org/10.1029/96jb00104

Zittel, W. D. (2019). *Theory and concept of operations for multi-PRF dealiasing algorithm's VCP 112* (Technical Report). NWS Radar Operations Center Applications Branch. Retrieved from https://www.roc.noaa.gov/WSR88D/PublicDocs/NewTechnology/Theory_ConOps_VCP112.pdf